Comparison of a Very-fine-resolution GCM with RCM Dynamical Downscaling in Simulating Climate in China

Donglin GUO[*1] and Huijun WANG[1,2,3]

[1]*Nansen-Zhu International Research Center, Institute of Atmospheric Physics, Chinese Academy of Sciences, Beijing* 100029
[2]*Climate Change Research Center, Chinese Academy of Sciences, Beijing* 100029
[3]*Collaborative Innovation Center on Forecast and Evaluation of Meteorological Disasters,*
Nanjing University of Information Science & Technology, Nanjing 210044

ABSTRACT

Regional climate simulation can generally be improved by using an RCM nested within a coarser-resolution GCM. However, whether or not it can also be improved by the direct use of a state-of-the-art GCM with very fine resolution, close to that of an RCM, and, if so, which is the better approach, are open questions. These questions are important for understanding and using these two kinds of simulation approaches, but have not yet been investigated. Accordingly, the present reported work compared simulation results over China from a very-fine-resolution GCM (VFRGCM) and from RCM dynamical downscaling. The results showed that: (1) The VFRGCM reproduces the climatologies and trends of both air temperature and precipitation, as well as inter-monthly variations of air temperature in terms of spatial pattern and amount, closer to observations than the coarse-resolution version of the GCM. This is not the case, however, for the inter-monthly variations of precipitation. (2) The VFRGCM captures the climatology, trend, and inter-monthly variation of air temperature, as well as the trend in precipitation, more reasonably than the RCM dynamical downscaling method. (3) The RCM dynamical downscaling method performs better than the VFRGCM in terms of the climatology and inter-monthly variation of precipitation. Overall, the results suggest that VFRGCMs possess great potential with regard to their application in climate simulation in the future, and the RCM dynamical downscaling method is still dominant in terms of regional precipitation simulation.

Key words: climate simulation, dynamical downscaling, GCM, RCM

Citation: Guo, D. L., and H. J. Wang, 2016: Comparison of a very-fine-resolution GCM with RCM dynamical downscaling in simulating climate in China. *Adv. Atmos. Sci.*, **33**(5), 559–570, doi: 10.1007/s00376-015-5147-y.

1. Introduction

Following the development of RCM dynamical downscaling (Dickinson et al., 1989; Giorgi and Bates, 1989; Giorgi, 1990), the method is now widely used to simulate regional climate in many different regions worldwide. This is mainly due to its more realistic topographic forcings, comprehensive physical processes, and the related improvement in simulation results relative to the driving GCM (Ju et al., 2007; Yu et al., 2010, 2015; Gao et al., 2012; Endris et al., 2013; Martynov et al., 2013). The method appears to be more effective for regions with complex topography, such as China, characterized by its wide variety of highly different landscapes, with the Tibetan Plateau and various mountain chains in the west and the north and lower lands in the east (Gao et al., 2008). Ju et al. (2007) simulated the East Asian climate at the Last Glacial Maximum (LGM) using RegCM2 (Giorgi et al., 1993a, 1993b) nested within an atmospheric GCM, and proved that the high-resolution RegCM2 can capture additional regional details of the LGM climate. When RegCM3 (Pal et al., 2007) was nested within the global model FvGCM [finite volume general circulation model (Lin and Rood, 1996; Kiehl et al., 1996)], Gao et al. (2008) found that it showed a better performance in both the spatial pattern and amount of precipitation over East Asia than FvGCM alone, with the most marked improvement being the removal of an artificial precipitation center over the eastern edge of the Tibetan Plateau. Recently, the WRF model (Skamarock et al., 2008) model was employed to simulate changes in climate extremes over China. Driven by MIROC5 (Hasumi and Emori, 2004) from CMIP5 (Coupled Model Intercomparison Phase 5) (Yu et al., 2015), it was found that WRF can better reproduce the main features of the climate extremes compared with MIROC5 (Yu et al., 2015).

However, as funding sources to develop climate models have increased, the horizontal resolutions of GCMs have become finer. For instance, in CMIP5, some modeling centers have provided higher resolution simulation results relative to in CMIP3, such as the results from MIROC4h (Sakamoto et

---

* Corresponding author: Donglin GUO
   Email: guodl@mail.iap.ac.cn

al., 2012) and BCC_CSM1.1(m) (Wu et al., 2010). The horizontal resolution of MIROC4h is approximately $0.5625° \times 0.5625°$, which is close to the level of RCM dynamical downscaling methods (Gao et al., 2013; Wang and Yu, 2013a). In the AMIP (Atmospheric Model Intercomparison Project), some models have a horizontal resolution less than 50 km, e.g., MRI-AGCM (Mizuta et al., 2012) and NICAM [Nonhydrostatic Icosahedral Atmospheric Model (Kodama et al., 2015)]. Thus, the question arises as to whether these very-fine-resolution GCMs (VFRGCMs) threaten the advantage of high-resolution RCM dynamical downscaling. Attempting to address this question is highly important for understanding and using these two kinds of simulation approaches in the future.

The objectives of the present study were to: (1) compare the simulation of a VFRGCM with that of its coarse-resolution version over China, and (2) compare the VFRGCM simulation to an RCM dynamical downscaling simulation over China under an almost equal horizontal resolution. Observational data were also used for comparison purposes. In section 2, brief descriptions of the data and models are provided. Section 3 compares the climatologies, trends, and inter-monthly variations of temperature and precipitation in the three simulations. Further discussion on the discrepancies between the RCM dynamical downscaling and VFRGCM simulations is provided in section 4. A summary of the key findings is presented in section 5.

2.   Model, observations, and methods

2.1.   *Model*

The coarse-resolution GCM used in this study was MIROC3.2 (hires) (hereafter, M3H), developed by the Center for Climate System Research, National Institute for Environmental Studies, and Frontier Research Center for Global Change of Japan (Hasumi and Emori, 2004). The horizontal resolution of the atmospheric model is approximately $1.125° \times 1.125°$. The height of the model top is about 40 km, having 56 vertical σ layers with relatively finer vertical resolution in the planetary layer and around the tropopause. The land surface model is MATSIRO (Minimal Advanced Treatments of Surface Interaction and RunOff) (Takata et al., 2003). The model has one canopy layer, five soil layers, and a variable number (0–3) of snow layers. The total thickness of the soil layer is 2 m. The ocean model has 47 vertical levels, and the vertical coordinate is a hybrid of σ and z. The horizontal resolution of the ocean model is approximately $0.28125°$ (lon) $\times 0.1875°$ (lat). As a component of CMIP3, M3H has carried out historical simulations of the period 1850–2000, using observed natural and anthropogenic forcings (Nozawa et al., 2007): changes in total solar irradiance (Lean et al., 1995), volcanic aerosols (Sato et al., 1993), well-mixed greenhouse gases (Johns et al., 2003), tropospheric and stratospheric ozone (Randel and Wu, 1999; Sudo et al., 2002), surface emissions of anthropogenic carbonaceous aerosols (Nozawa and Kurokawa, 2006) and pre-

cursors of sulfate aerosols (Lefohn et al., 1999), and land use (Hirabayashi et al., 2005). The simulation results have been widely used to analyze global or regional climate change and to drive RCMs (Lucarini et al., 2007; Gao et al., 2012; Guo et al., 2014).

The VFRGCM used in this study was MIROC4h (hereafter, M4H), which was developed as an improved version of M3H (Sakamoto et al., 2012). The height of the atmospheric model top and its vertical σ layers and resolution are the same as those of M3H. The land surface model as well as the vertical coordinate, vertical levels and horizontal resolution of the ocean model are also the same as those in M3H. The most fundamental change in M4H, compared to M3H, is a doubling of the horizontal resolution of the atmospheric model to approximately $0.5625°$. Additionally, a minor change from M3H to M4H is the difference in the latitude where the isopycnal layer thickness diffusion is applied in the Northern Hemisphere (Sakamoto et al., 2012). As a component of CMIP5, M4H has carried out historical simulations of the period 1950–2006 using almost the same observed natural and anthropogenic forcings as M3H, except for surface emissions of anthropogenic carbonaceous aerosols and sulfate aerosols [M3H used the data from Lefohn et al. (1999) and Nozawa and Kurokawa (2006) while M4H used the data from Lamarque et al. (2010)]. Sakamoto et al. (2012) found that M4H achieves many improvements in climate simulation compared with M3H, including not only smaller errors in the reproducibility of the surface variables, but also more realistic results for the interannual effects of events such as ENSO. These improvements are mostly due to the use of a higher resolution atmospheric model in M4H (Sakamoto et al., 2012).

The RCM dynamical downscaling simulation was carried out using WRF-ARW, version 3.3.1 (Skamarock et al., 2008), driven by the output of M3H. The microphysics scheme was WSM6 (Hong and Lim, 2006). The atmospheric radiation transfer schemes for longwave and shortwave radiation were calculated by CAM3.0 (Collins et al., 2004). The cumulus convective precipitation was parameterized by the Kain–Fritsch scheme (Kain, 2004). The planetary boundary layer was depicted by the Yonsei University scheme (Hong et al., 2006). The land surface model employed the Noah land surface model with multi-parameterization options (Niu et al., 2011). Notably, different sets of physical options may produce different simulated results (Yu et al., 2011). In this study, the above set was chosen because it can produce highly reasonable results for both air temperature and precipitation in China (Wang and Yu, 2013b). The period of simulation was 1980 to 2000, and the first year of the period was taken as the spin-up phase. The horizontal resolution of the simulation was 50 km (approximately $0.5°$), with 23 vertical layers from the surface up to a model top at 50 hPa. The simulation domain covered all of China and its surrounding areas, including 164×128 (east–west $\times$ north–south) grid points, with the center at (35° N, 102° E) (Fig. 1c). More detailed information can be found in the works of Wang and Yu (2013a, b).
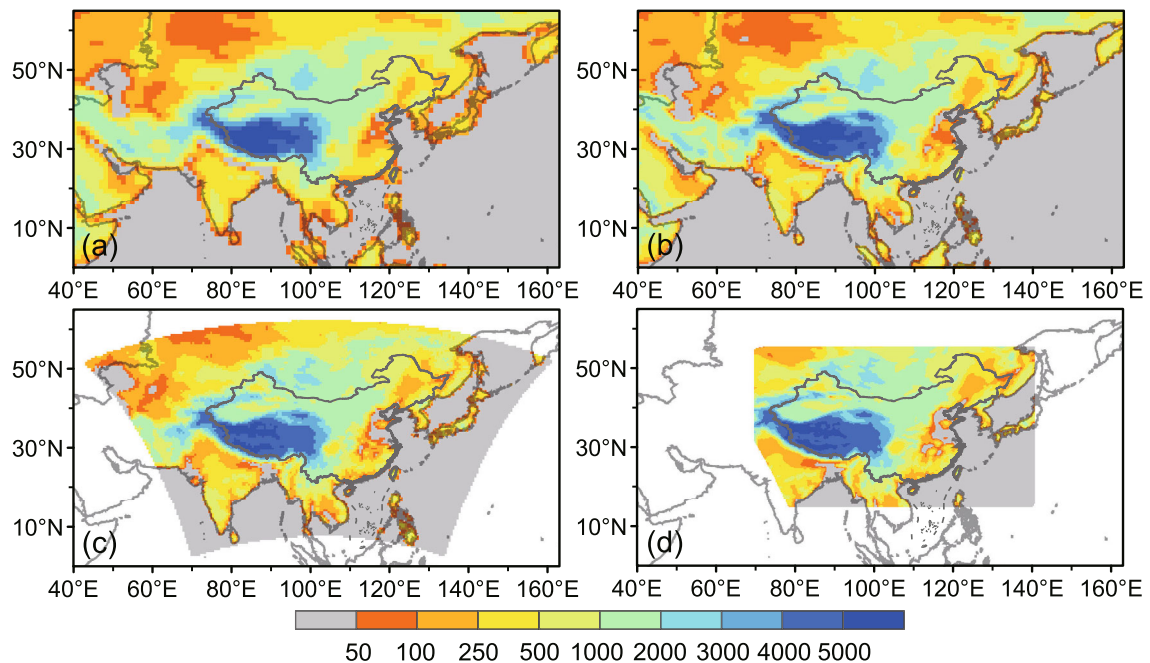
Fig. 1. The topographies (m) used in (a) M3H, (b) M4H, (c) WRF, and (d) CN05.1. The simulation domain for WRF is also shown in (c).

2.2. *Observations*

The CN05.1 dataset is an upgraded version of the previous dataset, CN05 (Xu et al., 2009), and was used as the observation in this study to compare with the simulation results. The dataset contains daily mean temperature, maximum temperature, minimum temperature, precipitation, evaporation, mean wind speed, and relative humidity, at a horizontal resolution of $0.25° \times 0.25°$, and covers the period from 1961 to 2012. The product was developed by increasing the number of stations, in China, used in the interpolation of observations, from 751 in CN05 to 2416 in CN05.1, and was obtained from the China Meteorological Administration (Wu and Gao, 2013). The data are reliable and have been widely used as an appropriate reference for comparisons with simulation results (Guo and Wang, 2013, 2014; Ma et al., 2015; Yu et al., 2015).

2.3. *Methods*

In order to perform a homogenous comparison, all data from M3H, M4H and WRF were interpolated into a common resolution of $0.25° \times 0.25°$, which is the same as that of the CN05.1 data. The influence of topography on simulated temperature were corrected during the process of interpolation. The specific method for the correction was that the original coarser resolution simulated temperature was firstly converted into values at sea level (0 m height), based on the corresponding coarser resolution topography and vertical temperature lapse rate [$(0.65°C (100 m)^{-1}$], and then those values were horizontally interpolated into the higher resolution data using a bilinear interpolation method. Finally, they were again converted into the temperature at the correspond-

ing higher resolution topography, based on the vertical temperature lapse rate. The trend was calculated using ordinary least-squares regression by deriving the slope of the linear fit, and its statistical significance was assessed using the Student's t-test method.

3. Results

In this section, the impact of topographic correction on the simulation results is firstly given, and then the simulation results from M3H, M4H and WRF are compared to the CN05.1 data in terms of the climatologies averaged for the period 1981–2000, trends during the period 1981–2000, and inter-monthly variations averaged for the period 1981–2000, for air temperature and precipitation, separately.

3.1. *Topographic correction*

The topographies used in M3H, M4H, WRF and CN05.1 are shown in Figs. 1a–d. It can be seen that the differences in the four sets of topographies are mainly situated on the Tibetan Plateau. The topography used in M3H is much higher on the Tibetan Plateau than that used in CN05.1; moreover, it fails to show some detailed information due to its coarser resolution. The topography used in M4H is still higher on the Tibetan Plateau than that used in CN05.1, but it shows greater regional detail relative to M3H. The topography used in WRF is quite similar to that used in CN05.1. These differences in topography indicate that topographic correction is necessary during the process of interpolating coarser resolution data into a higher resolution.
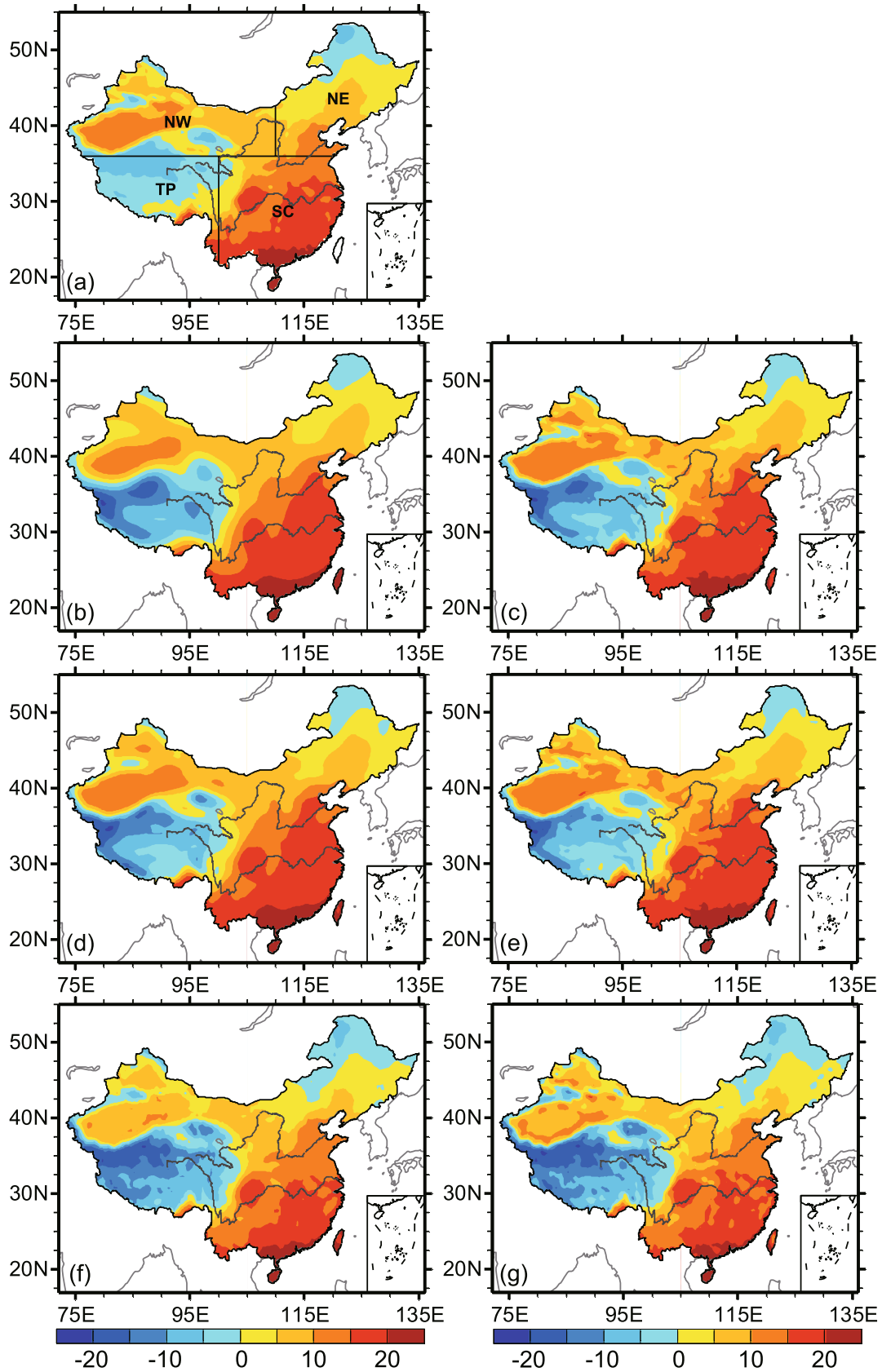
Fig. 2. Climatology of air temperature (°C) during the period 1981–2000 from (a) CN05.1, (b, c) MIROC3h, (d, e) MIROC4h, and (f, g) WRF. Panels (b, d, f) refer to the results without topographic correction, while (c, e, g) refer to the results with topographic correction. China was divided into four sub-regions [shown in (a)] for analysis, based on Shi (2010): northwestern China (NW); northeastern China (NE); the Tibetan Plateau (TP); South China (SC).

Figure 2 compares the results with and without topographic correction during the process of interpolation. It can clearly be seen that the air temperature from M3H becomes closer to observations after topographic correction is performed. The cold bias on the Tibetan Plateau becomes smaller, and many regional details in the Tibetan Plateau and northwestern China are present. For the entire region of China, the spatial correlation coefficient increases from 0.94 to 0.97 and the spatial RMSE decreases from 3.34°C to 2.80°C, after the topographic correction. The improvement is especially evident on the Tibetan Plateau; the spatial correlation coefficient increases from 0.88 to 0.92 and the spatial RMSE decreases from 6.28°C to 5.47°C (Table 1). The air temperature from M4H also improves after topographic correction. The spatial correlation coefficient increases from 0.96 to 0.97 and the spatial RMSE decreases from 2.87°C to 2.48°C (Table 1). In contrast, the air temperature from WRF shows very small changes after topographic correction, due to its close topography to that of CN05.1. These results suggest that topographic correction is necessary before comparing model results to observations.

3.2. *Climatology*

As shown in Figs. 2c, e and g, all three models capture the spatial pattern of the climatology of air temperature well, such as the high air temperature in southeastern China,

low air temperature in the Tibetan Plateau, and transitional temperature in northwestern, northeastern, and central China. Clearly, all three models give a lower temperature in the Tibetan Plateau compared to observations. This is especially true for WRF, which gives a distinctly lower temperature not only in the Tibetan Plateau but also in northwestern China (Fig. 2g). Relative to both M3H and WRF, M4H reproduces more realistic air temperature on the Tibetan Plateau, which is confirmed by the RMSE (root-mean-square error) of 5.23°C, relative to 6.28°C for M3H and 7.63°C for WRF (Table 1). For the entire region of China, M4H has an equal correlation coefficient of 0.97 with M3H and WRF, but the lowest RMSE of 2.48°C compared with 2.8°C for M3H and 3.99°C for WRF (Table 1). These results indicate that M4H is superior in simulating the climatology of air temperature in China.

For precipitation, all three models capture the gradually decreasing pattern from southeastern to northwestern China shown in observations (Figs. 3a–d). However, M3H and M4H yield an artificial precipitation center over the eastern edge of the Tibetan Plateau, although the center is smaller in M4H due to its more realistic topography (Figs. 3b and c). The center can also be seen in the WRF simulation results, but it is quite weak (Fig. 3d). Compared to M3H, the bias in the amount of precipitation is less in M4H because of the improved horizontal resolution. Compared to M4H, the WRF simulation is closer to observations in terms of both the spa-
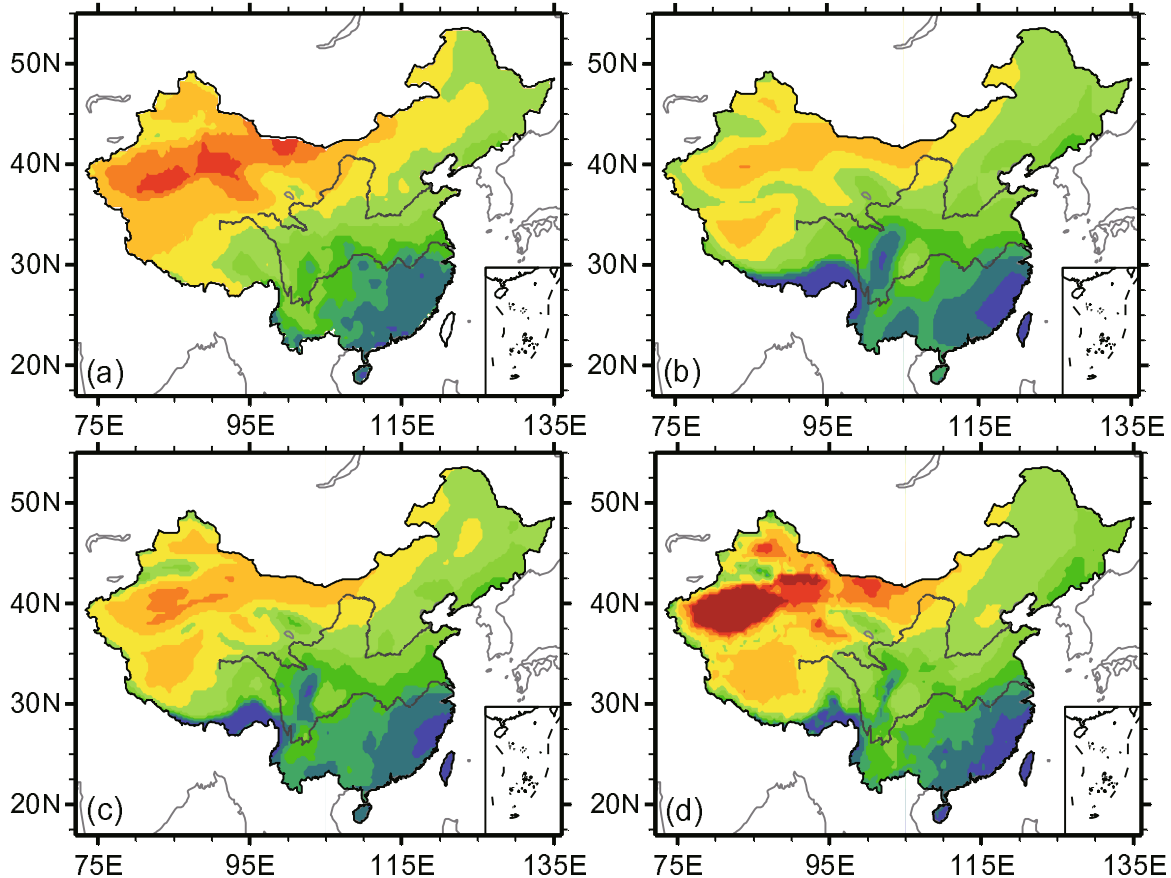

Fig. 3. Climatology of precipitation (mm yr^{-1}) during the period 1981–2000 from (a) CN05.1, (b) MIROC3h, (c) MIROC4h, and (d) WRF.

Table 1. Statistics of the similarities between the three simulated climatologies and trends in air temperature and precipitation during the period 1981–2000 and the corresponding CN05.1 data over China and the four sub-regions indicated in Fig. 2a. CC denotes spatial correlation coefficient, and all the correlation coefficients are statistically significant at the greater than 95% confidence level. For the temperature climatology, the values in brackets refer to the results without topographic correction.

	Temperature climatology		Trend in temperature		Precipitation climatology		Trend in precipitation	
	CC	RMSE ($°C$)	CC	RMSE [$°C$ $(10\ yr)^{-1}$]	CC	RMSE (mm d^{-1})	CC	RMSE [mm d^{-1} $(10\ yr)^{-1}$]
China								
M3H	0.97(0.94)	2.80(3.34)	−0.10	0.57	0.78	1.19	0.11	0.20
M4H	0.97(0.96)	2.48(2.87)	0.09	0.28	0.79	1.11	0.32	0.19
WRF	0.97(0.97)	3.99(3.91)	−0.05	0.65	0.89	0.78	0.32	0.21
Northwest								
M3H	0.97(0.86)	2.08(2.96)	−0.34	0.56	0.72	0.67	−0.04	0.05
M4H	0.97(0.94)	2.11(2.40)	0.24	0.15	0.82	0.52	0.37	0.04
WRF	0.95(0.93)	3.32(3.26)	−0.75	0.58	0.84	0.48	0.11	0.07
Northeast								
M3H	0.99(0.97)	1.57(1.63)	−0.19	0.63	0.88	0.46	0.09	0.14
M4H	0.99(0.98)	1.55(1.54)	0.52	0.38	0.88	0.36	0.24	0.13
WRF	0.98(0.98)	1.88(1.87)	−0.44	0.84	0.86	0.54	−0.16	0.20
Tibetan Plateau								
M3H	0.92(0.88)	5.47(6.28)	0.06	0.37	0.63	2.33	−0.19	0.19
M4H	0.91(0.90)	4.37(5.23)	−0.11	0.32	0.60	2.28	−0.05	0.20
WRF	0.97(0.96)	7.83(7.63)	0.43	0.52	0.67	1.36	0.18	0.20
South China								
M3H	0.99(0.96)	1.42(1.68)	−0.36	0.62	0.74	0.93	0.24	0.32
M4H	0.99(0.98)	1.67(1.87)	0.14	0.24	0.81	0.77	0.46	0.28
WRF	0.98(0.98)	1.62(1.60)	0.14	0.60	0.86	0.67	0.44	0.30

tial pattern and amount in all sub-regions except northeastern China, where M4H shows better performance (Table 1).

3.3. *Trends*

Observations show that almost all areas of China experienced an increasing trend in air temperature during the period 1981–2000, especially in the northern part of China (Fig. 4a). However, M3H yields a decreasing trend in many areas of China, such as in eastern and southern parts (Fig. 4c). The WRF dynamical downscaling based on M3H also yields a decreasing trend, in more areas of China than M3H (Fig. 4g). Notably, M4H shows a distinctly more reasonable result than M3H and WRF; the decreasing trends shown in many areas in M3H and WRF shift to increasing trends in M4H, closer to observations (Fig. 4e). For the entire region of China, the spatial RMSE of M4H is 0.28°C $(10\ yr)^{-1}$, which is much lower than the values of 0.57 and 0.65°C $(10\ yr)^{-1}$ for M3H and WRF, respectively (Table 1).

For precipitation, a clear north–south oriented pattern of positive–negative–positive change was observed in southern China (Fig. 4b). Of the three models, WRF is the most successful in reproducing this pattern (Fig. 4h). However, it fails to capture the positive center in central China [approximately (33° N, 107° E)], as well as the positive trend in northeastern China. In contrast, M4H successfully captures these two features shown in observations (Fig. 4f). For all regions of China, both M4H and WRF have equal spatial correlation co-

efficients with observations, but M4H has lower RMSE than WRF (Table 1). For four sub-regions, M4H also performs better than WRF in terms of the spatial correlation coefficient and RMSE, except for the Tibetan Plateau.

Area-averaged yearly time series of air temperature and precipitation from CN05.1 and the three models, as averaged over the entire region of China and four sub-regions during the period 1981–2000, are presented in Fig. 5. Because atmosphere–ocean coupled GCMs generally cannot reproduce past interannual variations of air temperature and precipitation, it may not be reasonable to directly compare the interannual variation of model results with observations. Therefore, only trends and biases of the area-averaged yearly time series were analyzed. For the entire region of China, the trend of air temperature from M4H is 0.39°C $(10\ yr)^{-1}$, which is in closest agreement with the observed result of 0.50°C $(10\ yr)^{-1}$, relative to 0.06 and −0.05°C $(10\ yr)^{-1}$ for M3H and WRF, respectively (Fig. 5). As for bias, apparently, WRF shows a considerable cold bias in spite of relatively small biases in M3H and M4H, compared to observations. For the four sub-regions, the trends of air temperature produced by M4H is the most consistent with observations. Notably, the air temperature produced by WRF shows a weaker performance than that of M3H, in terms of both trend and bias, in China as a whole and in the four sub-regions except for northwest China. In other words, RCM dynamical downscaling seems to increase the deviation between the driving
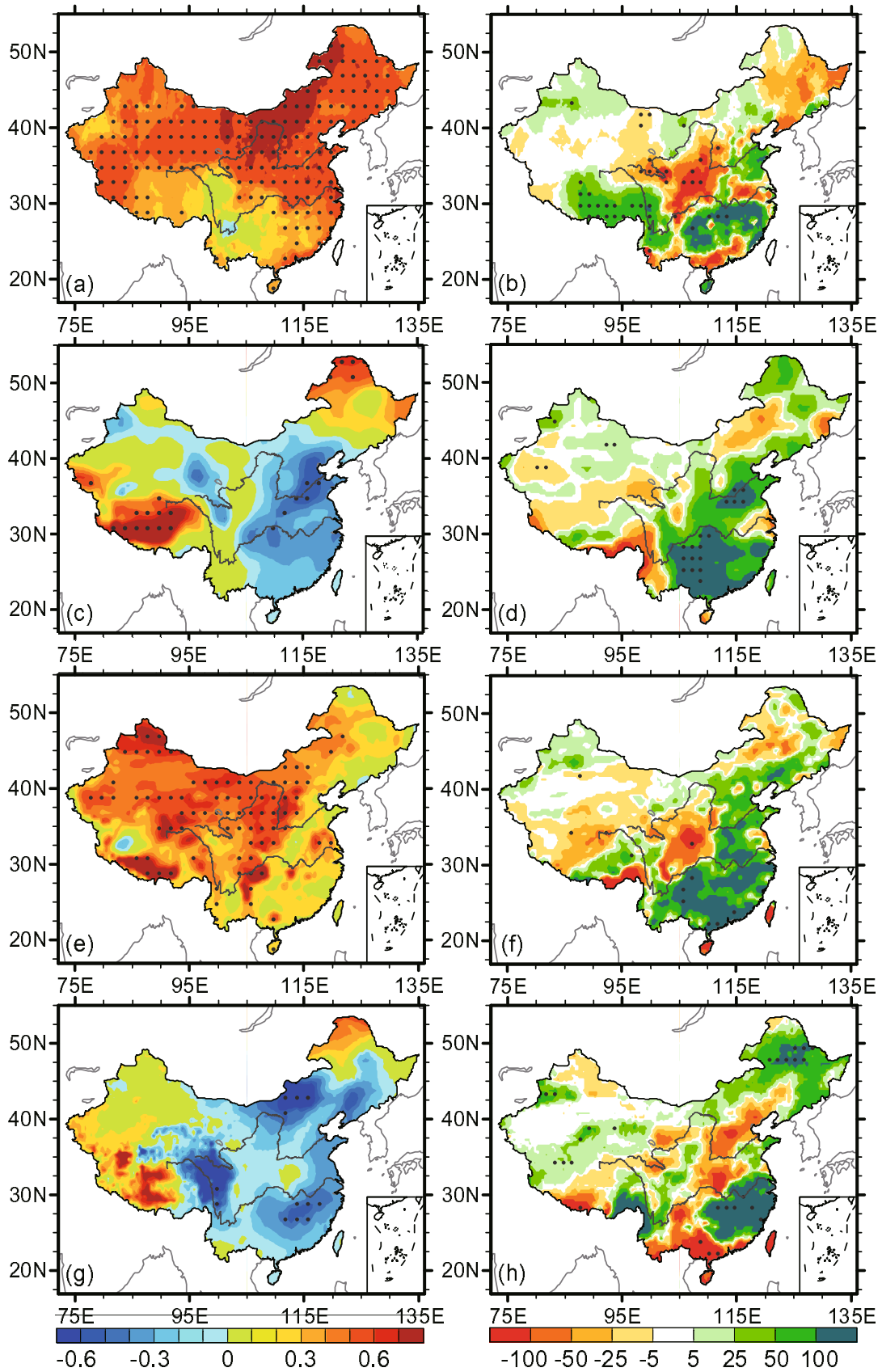
Fig. 4. Trends in (a, c, e, g) air temperature [°C (10 yr)$^{-1}$] and (b, d, f, h) precipitation [mm (10 yr)$^{-1}$] during the period 1981–2000 from (a, b) CN05.1, (c, d) MIROC3h, (e, f) MIROC4h, and (g, h) WRF. Areas with statistical significance exceeding the 95% confidence level are denoted by black dots.
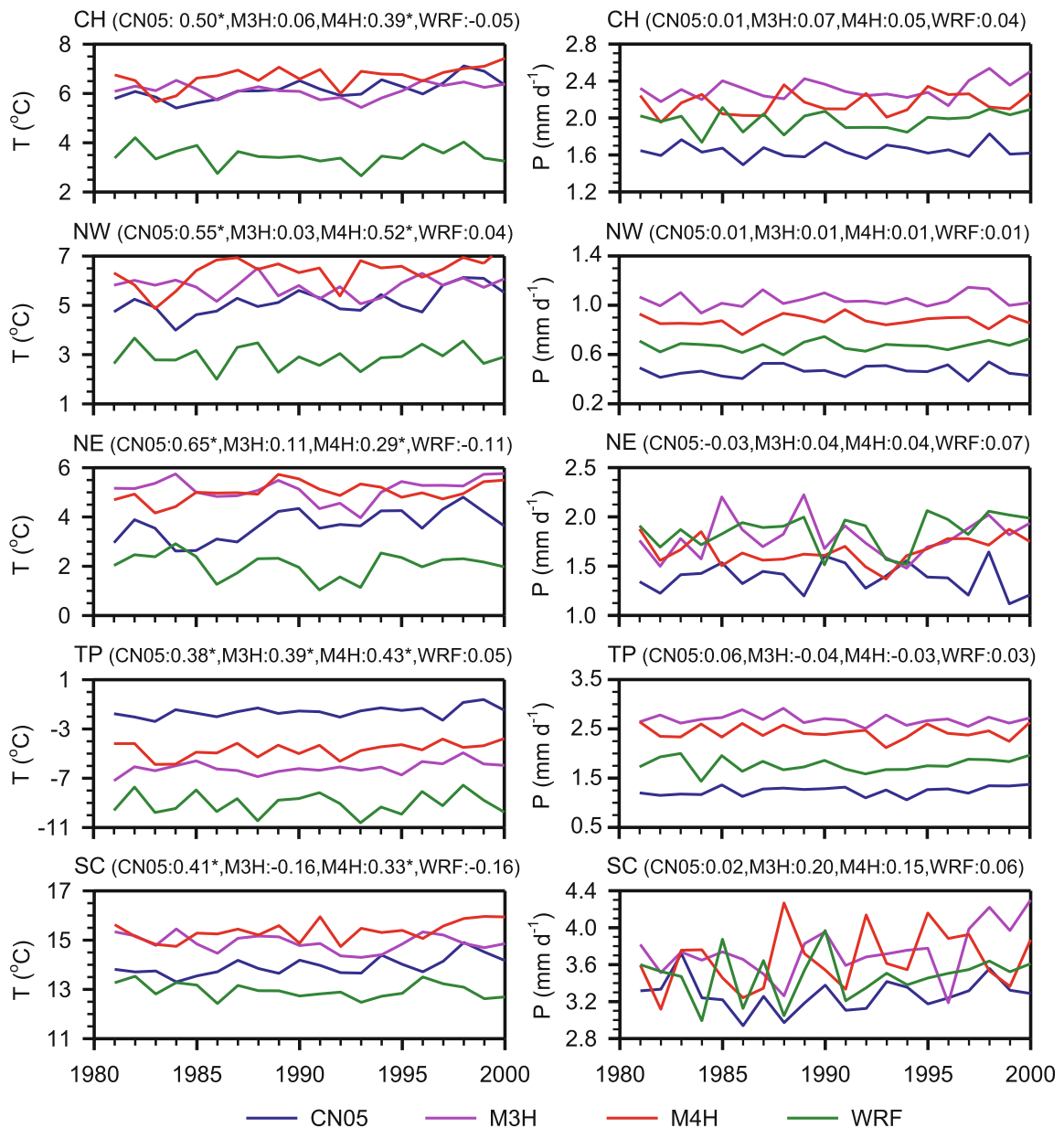
Fig. 5. Yearly time series of air temperature (T) and precipitation (P) change from CN05.1, MIROC3h (M3H), MIROC4h (M4H), and WRF during the period 1981–2000, as averaged over China and the four sub-regions indicated in Fig. 2a. The trends [units: °C $(10 \text{ yr})^{-1}$ for temperature and mm d^{-1} $(10 \text{ yr})^{-1}$ for precipitation] of each series are labelled at the top of each subgraph, and asterisks indicate statistical significance at the greater than 95% confidence level. Note: CH, NW, NE, TP, and SC denote China, northwestern China, northeastern China, the Tibetan Plateau, and South China, respectively.

GCM and observations. The possible reasons for this are discussed in section 4.

As shown in Fig. 5, M4H shows reduced bias and a closer trend with the observed time series of precipitation compared to M3H. In spite of this, WRF produces time series of precipitation that are in closest agreement with observations among the three models, in terms of both trend and bias, over all regions except northeastern China. These results indicate that the dynamical downscaling method can better improve the trend and bias of area-average time series of precipitation than a fine-resolution GCM.

3.4. *Inter-monthly variation*

Figure 6 shows time series of monthly air temperature and precipitation, as averaged during the period 1981–2000, from CN05.1 and the three models over the entire region of China and four sub-regions. All three models reproduce the observed inter-monthly variation of air temperature well over the entire region of China, as well as in northwestern, northeastern and southern China. The correlation coefficients are above 0.898. Over the Tibetan Plateau, the correlation coefficients are still high, but significant cold biases are apparent. M4H shows the closest agreement with the observed inter-
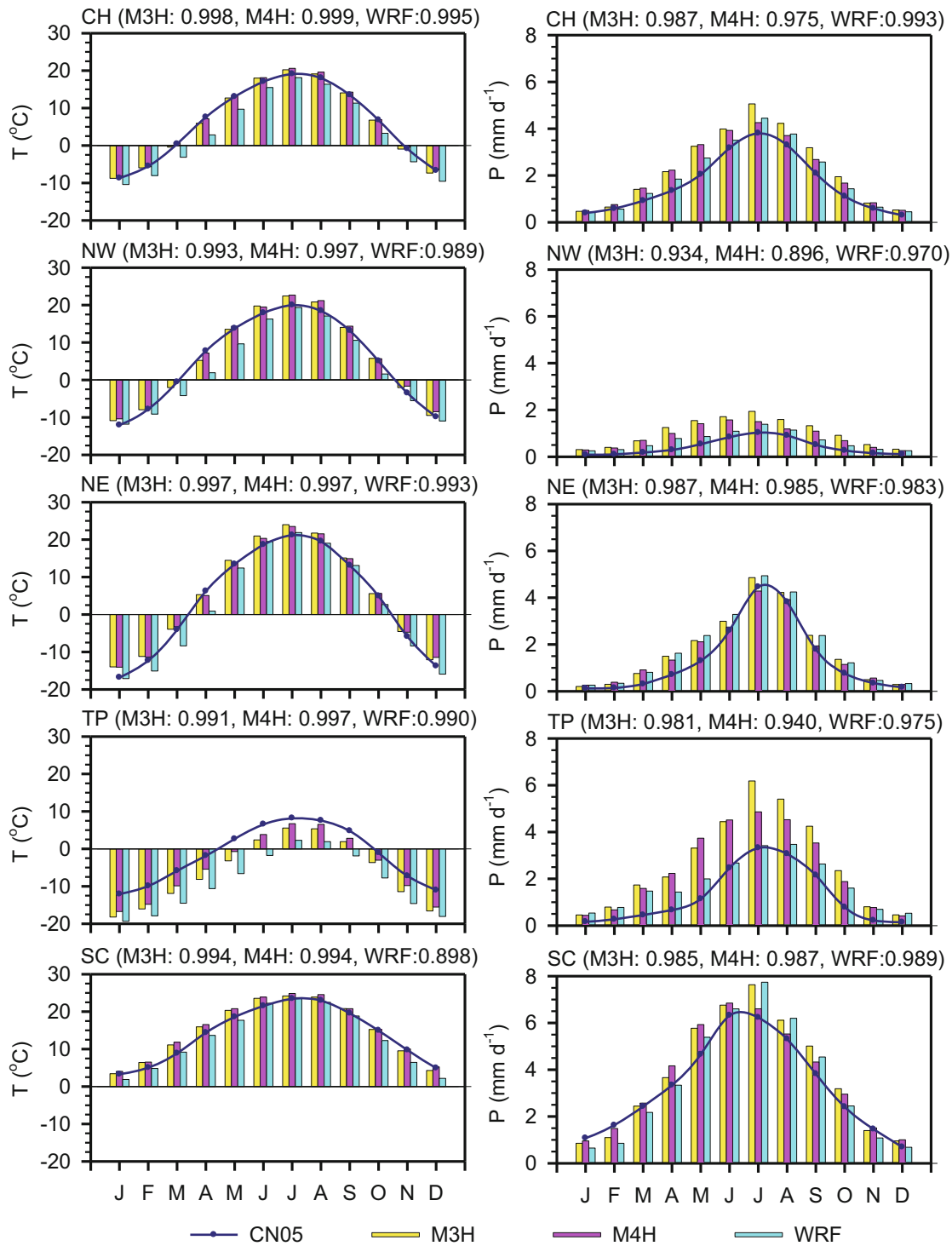
Fig. 6. Annual cycle of monthly averaged air temperature (T) and precipitation (P) from CN05.1, MIROC3h (M3H), MIROC4h (M4H), and WRF, as averaged during the period 1981–2000 over China and the four sub-regions indicated in Fig. 2a. The temporal correlation coefficients between the three simulated results and CN05.1 are labelled at the top of each panel, and all the correlation coefficients are statistically significant at the greater than 95% confidence level. Note: CN, NW, NE, TP, and SC denote China, northwestern China, northeastern China, the Tibetan Plateau, and South China, respectively.

monthly variation of air temperature among the three models, in terms of both correlation and bias, followed by M3H and WRF. These results are also true for all four sub-regions.

For precipitation, the correlations between the simulated monthly time series and observations are also high for all three models, over the entire region of China and the four sub-

regions, but with emerging large biases, relative to air temperature. Also, similar to the interannual variation of precipitation, WRF shows the closest agreement with the observed inter-monthly variation of precipitation among the three models, in terms of both correlation and bias, over all regions except northeastern China (Fig. 6). M4H shows distinctly lower correlation and larger bias with observations than WRF over all regions except northeastern China. Compared to M3H, M4H shows a reduced bias with observations over the entire region of China and the four sub-regions, but a lower correlation with observations over all regions except southern China (Fig. 6). The lower correlation of M4H with observations than M3H is a primary cause of the large discrepancy in correlations between M4H and WRF with observations.

4. Discussion

China is characterized by complex topography and unique weather and climate systems. A coarse-resolution GCM will usually produce considerable discrepancies against observations when simulating the climate in China, such as significantly lower air temperature but more precipitation over the Tibetan Plateau, an artificial precipitation center over the eastern edge of the Tibetan Plateau, and poor reproduction of regional details of climatic variables (Gao et al., 2008, 2013). With its advantages of more realistic topographic forcings and comprehensive physical processes, RCM dynamical downscaling is a method that offers great improvements to simulation results, such as a significant decrease in bias, better reproduction of regional details, and removal of the aforementioned artificial precipitation center (Gao et al., 2008; Wang and Yu, 2013b; Yu et al., 2015). The present study found that the simulation of climate in China can also be significantly improved by the direct use of a VFRGCM, i.e., a GCM that has a resolution almost equal to that of RCM dynamical downscaling. However, some differences between these two simulation approaches remain. The possible reasons for these differences are discussed in this section.

The VFRGCM used in the present work produced a more realistic climatology of air temperature than RCM dynamical downscaling. Furthermore, RCM dynamical downscaling showed a colder bias on average than the driving GCM. The high-resolution model might capture some land cover types, such as snow cover, glaciers, and permafrost. These land cover types melted and absorbed heat, thus resulting in cool air temperature. Because these land cover types may be small in area or isolated, they would not be captured by the coarse-resolution GCM, thus not resulting in the cool air temperature. This may partly explain the colder bias of RCM dynamical downscaling compared to the coarse-resolution GCM. However, if this is true, the VFRGCM should also show a colder bias than the coarse-resolution GCM, but this was not the case in our results. A further explanation could be that the cold bias of the VFRGCM may be offset by the heat from the wider region, such as the ocean. RCM dynamical down-

scaling is restricted to a smaller region and prescribed boundary conditions from coarse-resolution GCM, and thus its cold bias would not be adequately offset.

The VFRGCM used in the present work also produced a more realistic trend of air temperature than RCM dynamical downscaling. A reason for this difference may relate to the different data sources of anthropogenic carbonaceous aerosol and sulfate aerosol emissions used in M3H and M4H. As described in section 2.1, M3H uses the aerosol data from Lefohn et al. (2005) and Nozawa and Kurokawa (2006), while M4H uses aerosol data from Lamarque et al. (2010). This may also contribute to the differences in the air temperature trends between the VFRGCM and RCM. Another reason for this difference may relate to the higher climate sensitivity of M4H. Sakamoto et al. (2012) found that M4H has an effective climate sensitivity to a doubling CO_2 of 5.69°C, which is higher than the value 3.68°C for MIROC 3.2 (midres), and the range (2°C–4.5°C) of climate sensitivity reported in IPCC AR4 (Meehl et al., 2007). The higher climate sensitivity may also be one of the reasons for the differences between the air temperature trends from the VFRGCM and RCM. In addition, compared to VFRGCM, RCM has more complex model physical parameterizations, which will inevitably induce large model uncertainty. The uncertainty in model physics can evidently affect the simulated results (Yang et al., 2015a, 2015b). This may be one of the reasons for the more realistic trend of air temperature produced by the VFRGCM compared with RCM dynamical downscaling.

For precipitation, both the VFRGCM and RCM dynamical downscaling results showed reduced bias compared with the coarse-resolution GCM, due to their finer resolutions. However, RCM dynamic downscaling produced a smaller bias than the VFRGCM despite their almost equal horizontal resolutions. The differences may be attributable to the more comprehensive physical processes of the RCM dynamical downscaling approach compared with the VFRGCM (Yang et al., 2015a, 2015b).

Notably, all three models give a cold bias on the Tibetan Plateau compared to observations. This is especially true in the western part of the Tibetan Plateau. In general, it is thought that the cold bias results from the climate model. However, it should be noted that the CN05.1 data, used for comparison, include very sparse meteorological station data in the western part of the Tibetan Plateau (Wu and Gao, 2013). Therefore, it is possible that the CN05.1 data are somewhat inaccurate in the western part of the Tibetan Plateau, and this may contribute to the cold bias.

5. Conclusions

Climate simulations in China using a VFRGCM were compared to those based on RCM dynamical downscaling, each possessing almost equal horizontal resolution. Topographic correction can evidently improve GCM air temperature, and thus it should be required before comparing GCM air temperature to observations. Given the fine resolution of

the GCM, the climatology, trend, and inter-monthly variation of air temperature, as well as the climatology and trend of precipitation, obtained more reasonable results relative to its coarse-resolution version. However, the situation in terms of the inter-monthly variation of precipitation was different; the fine-resolution GCM showed a reduced bias but a lower correlation with observations compared to its coarse-resolution version. Compared to RCM dynamical downscaling, the VFRGCM better captured the climatology, trend, and inter-monthly variation of air temperature, as well as the trend in precipitation, in terms of the spatial pattern and amount, but showed weaker performance in simulating the climatology and inter-monthly variation of precipitation. As indicated by the results, for simulations of regional precipitation, RCM dynamical downscaling is still the dominant approach, but VFRGCMs possess great potential with regard to their application in climate simulations in the future.

The present reported results provide information on the differences between using GCMs with coarse and fine resolutions, which have same dynamical and physical processes, and dynamical downscaling from the same coarse-resolution GCM to simulate climate in China. They will be useful for understanding and using GCMs and RCMs to improve such simulations of climate in China in the future. Nevertheless, it should be stressed that these results are limited to the model chosen for use in this study, and differences may be found in the results of other models. Therefore, continued work is needed to compare the results from other models, and to explore the reasons for discrepancies between the simulations of VFRGCMs and RCM dynamical downscaling.

REFERENCES

Collins, W., and Coauthors, 2004: Description of the NCAR community atmosphere model (CAM 3.0). NCAR Tech Note NCAR/TN-464+STR, 214 pp.

Dickinson, R. E., R. M. Errico, F. Giorgi, and G. T. Bates, 1989: A regional climate model for the western United States. *Climatic Change*, **15**, 383–422.

Endris, H. S., and Coauthors, 2013: Assessment of the performance of CORDEX regional climate models in simulating East African rainfall. *J. Climate*, **26**, 8453–8475.

Gao, X., Y. Shi, R. Song, F. Giorgi, Y. Wang, and D. Zhang, 2008: Reduction of future monsoon precipitation over China: Comparison between a high resolution RCM simulation and the driving GCM. *Meteor. Atmos. Phys.*, **100**, 73–86.

Gao, X. J., Y. Shi, D. F. Zhang, and F. Giorgi, 2012: Climate change in China in the 21st century as simulated by a high resolution regional climate model. *Chinese Science Bulletin*, **57**, 1188–1195.

Gao, X. J., M. L. Wang, and F. Giorgi, 2013: Climate change

over China in the 21st century as simulated by BCC_CSM1.1-RegCM4.0. *Atmos. Oceanic Sci. Lett.*, **6**, 381–386.

Giorgi, F., 1990: Simulation of regional climate using a limited area model nested in a general circulation model. *J. Climate*, **3**, 941–964.

Giorgi, F., and G. T. Bates, 1989: On the climatological skill of a regional model over complex terrain. *Mon. Wea. Rev.*, **117**, 2325–2347.

Giorgi, F., M. R. Marinucci, and G. T. Bates, 1993a: Development of a second-generation regional climate model (RegCM2). Part I: Boundary layer and radiative transfer processes. *Mon. Wea. Rev.*, **121**, 2794–2813.

Giorgi, F., M. R. Marinucci, G. T. Bates, and G. D. Canio, 1993b: Development of a second-generation regional climate model (RegCM2). Part II: Convective processes and assimilation of lateral boundary conditions. *Mon. Wea. Rev.*, **121**, 2814–2832.

Guo, D. L., and H. J. Wang, 2013: Simulation of permafrost and seasonally frozen ground conditions on the Tibetan Plateau, 1981–2010. *J. Geophys. Res.*, **118**, 5216–5230.

Guo, D. L., and H. J. Wang, 2014: Simulated change in the near-surface soil freeze/thaw cycle on the Tibetan Plateau from 1981 to 2010. *Chinese Science Bulletin*, **59**, 2439–2448.

Guo, D. L., H. J. Wang, and D. Li, 2012: A projection of permafrost degradation on the Tibetan Plateau during the 21st century. *J. Geophys. Res.*, **117**, D05106, doi: 10.1029/2011JD 016545.

Hasumi, H., and S. Emori, 2004: K-1 model developers: K-1 coupled model (MIROC) description. K-1 Tech. Rep. 1, Cent. for Clim. Syst. Res., Univ. Tokyo, Tokyo, Japan, 34 pp.

Hirabayashi, Y., S. Kanae, I. Struthers, and T. Oki, 2005: A 100-year (1901–2000) global retrospective estimation of the terrestrial water cycle. *J. Geophys. Res.*, **110**, D19101, doi: 10.1029/2004JD005492.

Hong, S. Y., and J. O. J. Lim, 2006: The WRF single-moment 6-class microphysics scheme (WSM6). *Journal of the Korean Meteorological Society*, **42**, 129–151.

Hong, S. Y., Y. Noh, and J. Dudhia, 2006: A new vertical diffusion package with an explicit treatment of entrainment processes. *Mon. Wea. Rev.*, **134**, 2318–2341.

Johns, T. C., and Coauthors, 2003: Anthropogenic climate change for 1860 to 2100 simulated with the HadCM3 model under updated emissions scenarios. *Climate Dyn.*, **20**, 583–612.

Ju, L. X., H. J. Wang, and D. B. Jiang, 2007: Simulation of the Last Glacial Maximum climate over East Asia with a regional climate model nested in a general circulation model. *Palaeogeography, Palaeoclimatology, Palaeoecology*, **248**, 376–390.

Kain, J. S., 2004: The Kain-Fritsch convective parameterization: an update. *J. Appl. Meteor.*, **43**, 170–181.

Kiehl, J. T., J. J. Hack, G. B. Bonan, B. A. Boville, B. P. Breigleb, D. L. Williamson, and P. J. Rasch, 1996: Description of the NCAR Community Climate Model (CCM3). NCAR Technical Note, NCAR/TN-420+STR, 152 pp.

Kodama, C., and Coauthors, 2015: A 20-year climatology of a NICAM AMIP-type simulation. *J. Meteor. Soc. Japan*, **93**, 393–424, doi: 10.2151/jmsj.2015-024.

Lamarque, J. F., and Coauthors, 2010: Historical (1850–2000) gridded anthropogenic and biomass burning emissions of reactive gases and aerosols: Methodology and application. *Atmos. Chem. Phys.*, **10**, 7017–7039.

Lean, J., J. Beer, and R. Bradley, 1995: Reconstruction of solar

irradiance since 1610: Implications for climate change. *Geophys. Res. Lett.*, **22**, 3195–3198.

Lefohn, A. S., J. D. Husar, and R. B. Husar, 1999: Estimating historical anthropogenic global sulfur emission patterns for the period 1850–1990. *Atmos. Environ.*, **33**, 3435–3444.

Lin, S. J., and R. B. Rood, 1996: Multidimensional flux-form semi-Lagrangian transport schemes. *Mon. Wea. Rev.*, **124**, 2046–2070.

Lucarini, V., S. Calmanti, A. Dell'Aquila, P. M. Ruti, and A. Speranza, 2007: Intercomparison of the northern hemisphere winter mid-latitude atmospheric variability of the IPCC models. *Climate Dyn.*, **28**, 829–848.

Ma, J. H., H. J. Wang, and K. Fan, 2015: Dynamic downscaling of summer precipitation prediction over China in 1998 using WRF and CCSM4. *Adv. Atmos. Sci.*, **32**, 577–584, doi: 10.1007/s00376-014-4143-y.

Martynov, A., Laprise R., Sushama L., Winger K., Šeparović L., and B. Dugas, 2013: Reanalysis-driven climate simulation over CORDEX North America domain using the Canadian Regional Climate Model, version 5: model performance evaluation. *Climate Dyn.*, **41**, 2973–3005.

Meehl, G. A., and Coauthors, 2007: Global climate projections. *Climate Change 2007: The Physical Science Basis. Contribution of Working Group I to the Fourth Assessment Report of the Intergovernmental Panel on Climate Change*, S. Solomon, et al., Eds., Cambridge University Press, Cambridge, United Kingdom and New York, NY, USA, 747–845.

Mizuta, R., and Coauthors, 2012: Climate simulations using MRI-AGCM3.2 with 20-km grid. *J. Meteor. Soc. Japan*, **90A**, 233–258.

Niu, G. Y., and Coauthors, 2011: The community Noah land surface model with multiparameterization options (Noah-MP): 1. Model description and evaluation with local-scale measurements. *J. Geophys. Res.*, **116**(D12), D12109, doi: 10.1029/2010JD015139.

Nozawa, T., and J. Kurokawa, 2006: Historical and future emissions of sulfur dioxide and black carbon for global and regional climate change studies. CGER-Report, CGER/NIES, Tsukuba, Japan.

Nozawa T., T. Nagashima, T. Ogura, T. Yokohata, N. Okada, and H. Shiogama, 2007: Climate change simulations with a coupled ocean-atmosphere GCM called the model for interdisciplinary research on climate: MIROC. CGER-Report, CGER/NIES, Tsukuba, Japan, 79 pp.

Pal, J. S., and Coauthors, 2007: Regional climate modeling for the developing world: The ICTP RegCM3 and RegCNET. *Bull. Amer. Meteor. Soc.*, **88**, 1395–1409.

Randel, W. J., and F. Wu, 1999: A stratospheric ozone trends data set for global modeling studies. *Geophys. Res. Lett.*, **26**, 3089–3092.

Sakamoto, T. T., and Coauthors, 2012: MIROC4h—A new high-resolution atmosphere-ocean coupled general circulation model. *J. Meteor. Soc. Japan*, **90**, 325–359.

Sato, M., J. E. Hansen, M. P. McCormick, and J. B. Pollack, 1993:

Stratospheric aerosol optical depths, 1850-1990. *J. Geophys. Res.*, **98**, 22 987–22 994.

Shi, Y., 2010: A high resolution climate change simulation of the 21st century over East Asia by RegCM3. Ph. D dissertation, Institute of Atmospheric Physics, Chinese Academy of Science, 117 pp. (in Chinese)

Skamarock, W. C., and Coauthors, 2008: A description of the advanced research WRF Version 3. NCAR Tech. Note, TN-475+STR, 113 pp.

Sudo, K., M. Takahashi, J. Kurokawa, and H. Akimoto, 2002: CHASER: A global chemical model of the troposphere: 1. Model description. *J. Geophys. Res.*, **107**, 4339, doi: 10.1029/2001JD001113.

Takata, K., S. Emori, and T. Watanabe, 2003: Development of the minimal advanced treatments of surface interaction and runoff. *Globat Planet Change*, **38**, 209–222.

Wang, S. Z., and E. T. Yu, 2013a: Simulation and projection of changes in rainy season precipitation over China using the WRF model. *Acta Meteorologica Sinica*, **27**, 577–584.

Wang, S. Z., and E. T. Yu, 2013b: Dynamical downscaling simulation over China using the nested MIROC/WRF model. *Climatic and Environmental Research*, **18**, 681–692. (in Chinese)

Wu, J., and X. J. Gao, 2013: A gridded daily observation dataset over China region and comparison with the other datasets. *Chinese Journal of Geophysics*, **56**, 1102–1111. (in Chinese)

Wu, T. W., and Coauthors, 2010: The Beijing Climate Center atmospheric general circulation model: Description and its performance for the present-day climate. *Climate Dyn.*, **34**, 123–147.

Xu, Y., X. J. Gao, Y. Shen, C. H. Xu, Y. Shi, and F. Giorgi, 2009: A daily temperature dataset over China and its application in validating a RCM simulation. *Adv. Atmos. Sci.*, **26**, 763–772, doi: 10.1007/s00376-009-9029-z.

Yang, B., Y. C. Zhang, Y. Qian, A. N. Huang, and H. P. Yan, 2015a: Calibration of a convective parameterization scheme in the WRF model and its impact on the simulation of East Asian summer monsoon precipitation. *Climate Dyn.*, **44**, 1661–1684.

Yang, B., Y. C. Zhang, Y. Qian, T. W. Wu, A. N. Huang, and Y. J. Fang, 2015b: Parametric sensitivity analysis for the Asian summer monsoon precipitation simulation in the Beijing Climate Center AGCM version 2.1. *J. Climate*, **28**, 5622–5644.

Yu, E. T., H. J. Wang, and J. Q. Sun, 2010: A quick report on a dynamical downscaling simulation over China using the nested model. *Atmos. Oceanic Sci. Lett.*, **3**, 325–329.

Yu, E. T., H. J. Wang, Y. Q. Gao, and J. Q. Sun, 2011: Impacts of cumulus convective parameterization schemes on summer monsoon precipitation simulation over China. *Acta Meteorologica Sinica*, **25**, 581–592.

Yu, E. T., J. Q. Sun, H. P. Chen, and W. L. Xiang, 2015: Evaluation of a high-resolution historical simulation over China: Climatology and extremes. *Climate Dyn.*, **45**, 2013–2031.